International Journal of Nanomedicine

Dovepress
Taylor & Francis Group

Open Access Full Text Article

ORIGINAL RESEARCH

Layered Double Hydroxide Nanoparticles Loaded with Resveratrol Inhibit Glycolysis and Show Efficacy in the Treatment of Breast Cancer

Chenchen Geng[1,2], Liuyang Yan[1,2], Yunhao Li[1,3], Houcong Li[1,3], Yuxin Ji[1,4], Yuhan Xiao[1,4], Zhifa Wang[1,2], Xiaoqi Chen[1], Changjie Chen[1,4,5], Qingling Yang[1,4,5], Baoding Tang[1,2,6], Wenrui Wang[1,2,6]

[1]Anhui Provincial Key Laboratory of Tumor Evolution and Intelligent Diagnosis and Treatment, Bengbu Medical University, Bengbu, Anhui, People's Republic of China; [2]School of Life Sciences, Bengbu Medical University, Bengbu, Anhui, People's Republic of China; [3]School of Basic Courses, Bengbu Medical University, Bengbu, Anhui, People's Republic of China; [4]Clinical Testing and Diagnose Experimental Center, Bengbu Medical University, Bengbu, Anhui, People's Republic of China; [5]Department of Biochemistry and Molecular Biology, Bengbu Medical University, Bengbu, Anhui, People's Republic of China; [6]Anhui Engineering Research Center for Neural Regeneration Technology and Medical New Materials, Bengbu Medical University, Bengbu, Anhui, People's Republic of China

Correspondence: Wenrui Wang; Baoding Tang, Anhui Provincial Key Laboratory of Tumor Evolution and Intelligent Diagnosis and Treatment, Bengbu medical university, 2600 Donghai Avenue, Bengbu, Anhui, 233030, People's Republic of China, Email wenrui-wang1983@163.com; baodtang_16@163.com

Background: Breast cancer is one of the most common cancers among women. Tumor cell proliferation is highly dependent on aerobic glycolysis, so regulating aerobic glycolysis in breast cancer cells is a promising therapeutic strategy. Resveratrol (Res), as a potential new anti-breast cancer drug, has been shown to regulate the glycolysis of cancer cells and inhibit the metastasis and recurrence of breast cancer. The nano drug delivery system can regulate the aerobic glycolysis metabolism by targeting the signaling factors and reaction products of the tumor aerobic glycolysis process to enhance the anti-tumor effect.

Methods: A new albumin-modified layered double hydroxide resveratrol dosage form (BSA@LDHs-Res) was synthesized by hydrothermal co-precipitation. Characterization was carried out to determine the successful synthesis of the nanocarrier system. The bioactivity, glycolytic activity and biocompatibility were examined by in vitro cellular assays; in vivo experiments were performed to further evaluate the anti-tumor effects of the BSA@LDHs-Res dosage form for breast cancer.

Results: In this study, we obtained for the first time a bovine serum albumin-modified BSA@LDHs-Res loaded dosage form, which was able to enter breast cancer cells SKBR3 and MDA-MB-231 via endocytosis and successfully escaped from lysosomal capture. BSA@LDHs-Res inhibited the proliferation, migration, and invasion of two types of breast cancer cells, induced apoptosis, and promoted the reduction of mitochondrial membrane potential and ROS. BSA@LDHs-Res inhibited the expression and viability of the key enzymes of glycolysis, hexokinase 2 (HK2), pyruvate kinase (PK), and lactate dehydrogenase, resulting in decreased glucose consumption, decreased lactate accumulation, and decreased intracellular ATP levels. BSA@LDHs-Res was examined in the mouse model with good anti-tumor effects.

Conclusion: BSA@LDHs-Res is an efficient nanoreagent for the treatment of breast cancer. The albumin-modified resveratrol layered double hydroxide delivery system developed in this study will provide some theoretical references for further research and clinical application of tumor aerobic glycolysis.

Keywords: layered double hydroxides, glycolysis, resveratrol, BSA

Introduction

Female breast cancer is the second leading cause of global cancer incidence in 2022, with an estimated 2.3 million new cases, and it poses a significant threat to women's health worldwide.[1] Breast cancer is classified into four sub-types, the most aggressive of which is human epidermal growth factor receptor 2 (HER2)-positive and more likely to metastases. This patient population requires costly, targeted therapies.[2] Triple-negative breast cancers, the most malignant breast cancer sub-type, accounts for 85% of basal-like breast cancers and is currently treated with radiotherapy.[3] Surgery, radiotherapy, and chemotherapy are the traditional treatments for breast cancer. However, one of the most severe clinical

Received: 18 September 2024
Accepted: 19 February 2025
Published: 17 March 2025

issues in breast cancer treatment is the high risk of recurrence and eventual drug resistance. Conventional radiotherapy regimens are no longer the best option for patients because they reduce long-term survival and are highly resistant to treatment.[4] Therefore, we urgently need to develop highly effective and low-toxicity breast cancer therapies, as well as continue to innovate and investigate new breast cancer treatment strategies.

Aerobic glycolysis is a well-recognized characteristic of cancer cell energy metabolism, known as the Warburg effect. Even in the pxresence of abundant oxygen, a majority of tumor cells produce substantial amounts of energy through a high glycolytic metabolism. Thus, inhibiting aerobic glycolysis in breast cancer cells has gradually become a popular research topic.[5] Enhanced glycolysis-related enzyme activity can promote tumor development and metastasis, and some drugs may inhibit the glycolytic pathway, making them potential anti-tumor targets.[6]

Resveratrol has been found to inhibit glycolysis in breast cancer cells, notably by suppressing the activity of 6-phosphofructo-1-kinase (PFK-1), a crucial enzyme in the glycolytic pathway. This inhibition reduces the energy supply of cancer cells, thereby suppressing tumor growth.[7] In addition to its direct impact on glycolysis, resveratrol also exhibits anti-proliferative and anti-metastatic effects, which include the inhibition of cell proliferation, reduction in cell vitality, and the suppression of invasion and metastasis in breast cancer treatment.[8] These effects are likely related to its modulation of the glycolytic pathway, suggesting that resveratrol can weaken the proliferation and survival ability of breast cancer cells, and suppress their growth and metastasis.[9–11] Furthermore, resveratrol has shown synergistic effects when used in combination with other chemotherapeutic drugs such as docetaxel, paclitaxel, cisplatin, and doxorubicin, potentially enhancing their anti-cancer properties against breast cancer cells.[12] This synergism may also be related to its regulation of the glycolytic pathway, offering a promising direction for combination therapies in breast cancer treatment. However, the poor water solubility, low bioavailability, rapid metabolism, and systemic elimination pf resveratrol limit its efficacy.[13] Therefore, we must optimise its bioavailability to ensure effective and stable action in breast cancer cells.

Nano drug delivery system is a hot research topic in recent years because it can improve the solubility of difficult-to-solve drugs, enhance the bioavailability of drugs, and have significant advantages in drug delivery. Some studies have shown that mesoporous silica nanoparticles (MSN-RSV) loaded with resveratrol can effectively inhibit the proliferation, migration and invasion of gastric cancer cells, and have significant anticancer effects.[14] It was also shown that resveratrol could be successfully loaded into solid lipid nanoparticles (Res-SLNs) for breast cancer treatment.[15] Layered double hydroxides (LDHs) are emerging as an exceptional inorganic matrix for biomedical applications, particularly in the realm of drug delivery. These synthetic cationic clay materials possess a brucite-like structure composed of hydroxide layers, wherein some divalent cations are replaced by trivalent ions, endowing the material with a positive charge. This charge allows the LDHs to interact with anions and hydrogen-bonded water molecules within the interlayer spacing, resulting in a versatile composition formula of represent a divalent cation, a trivalent metal cation, and an anion, respectively. LDHs are generally considered non-toxic and biocompatible, which is essential for pharmaceutical applications. LDHs can be functionalized with specific ligands to target resveratrol to particular cells or tissues, increasing the drug's efficacy and reducing side effects. LDHs can be combined with other therapeutic agents or imaging agents, offering potential for the development of theranostic systems. A multitude of researchers, including our research group, have carried out work in the area of utilizing layered double hydroxides to encapsulate natural drugs, altering their pharmaceutical forms for anti-tumor research in the preliminary stages.[16–18]

In the present study, we utilized bovine serum albumin-coated layered double hydroxides (BSA@LDHs) to encapsulate resveratrol, thereby overcoming the aforementioned limitations in its application. BSA@LDHs offer a promising platform for the delivery of resveratrol, resveratrol is sensitive to degradation, but encapsulation in LDH nanomaterials can protect it from environmental factors, enhancing its stability. BSA@LDHs can provide a controlled release mechanism for resveratrol, which is crucial for maintaining therapeutic concentrations over time. BSA@LDHs-Res can efficiently and stably deliver RES to the tumor site, enhancing its effectiveness against the tumor. This formulation reduces the expression of glucose transporter proteins in tumor cells, thereby cutting off the glucose supply and blocking the energy supply upstream of glycolysis. Additionally, it inhibits the glycolysis of breast cancer cells by regulating the activity of key downstream enzymes involved in glycolysis. Furthermore, BSA@LDHs-Res can induce apoptosis in breast cancer cells to a certain extent, contributing to its anti-breast cancer effects. The results of both in vitro and in vivo experiments indicate that the BSA@LDHs-Res nanocarrier system holds promising potential for application in breast cancer treatment.

Materials and Methods

$MgCl_2·6H_2O$ (97%), $AlCl_3·9H_2O$ (97%), NaOH (97%), and Resveratrol (≥98%) were purchased from Aladdin Reagent Co. Ltd (Shanghai, China); Bovine serum albumin (BSA) was purchased from Bio sharp Biologicals (Guangzhou, China); and DMEM (high glucose), DMEM/F12 and fetal bovine serum (FBS) were purchased from Thermo Fisher Biochemical Products Co., (Beijing, China); DMSO, BCA protein assay, SDS-PAGE and JC-1 mitochondrial membrane potential assay kits were purchased from Beyotime Biotechnology (Jiangsu, China). GLUT1 (1:800), HK2 (1:10,000) and PKM2 (1:2000), β-Actin (1:10,000) were purchased from Proteintech (USA); Horseradish peroxidase (HRP)-labeled goat anti-rabbit antibody (1:6000) was purchased from Affinity Bioscience (Nanjing, China). Annexin V-FITC/PI were purchased from Best Bio Biologicals (Shanghai, China); glucose kit, lactate kit, lactate dehydrogenase kit were purchased from Solar Biologicals (Beijing, China) Co. Ltd; ROS detection kit and ATP detection kit were purchased from Baxter (Nanjing, China) Bioscience Co.

HER2-positive breast cancer cell line SKBR3, triple-negative breast cancer cell line MDA-MB-231 and human normal breast epithelial cell MCF-10A were purchased from Shanghai Institute of Biochemistry and Cell Biology, Chinese Academy of Sciences. All cell lines used in the experiments were cultured at 37 °C under 5% CO_2 constant humidity. SKBR3 cells and MDA-MB-231 cells were cultured in DMEM culture medium containing 10% FBS. MCF-10A cells were cultured in DMEM/F12 medium containing 5% horse serum. All media used in the experiments were supplemented with 100 μg/mL streptomycin, 100 μg/mL penicillin, 100 μg/mL furazolidone and 100 μg/mL furacilin. Female BALB/c nude mice (5 weeks old) were purchased from Changzhou Cavins Laboratory Animal Co. Animal licence No. (SCXK(SU)2021–0013). They were housed in a SPF animal house at 25°C with relative humidity maintained at 40%-70%. All animal experiments were approved by the Animal Care and Use Committee of Bengbu Medical College (Ethics No. [2022] No. 147). All animal experiments were conducted in accordance with the Guide for the Care and Use of Laboratory Animals.

Synthesis of Mg-Al-LDHs, BSA@LDHs and BSA@LDHs-Res Nanoparticles

Calculate the mass of magnesium chloride ($MgCl_2·6H_2O$) and aluminum chloride ($AlCl_3·9H_2O$) based on the molar ratio of Mg^{2+} to Al^{3+} of 3:1. Prepare 10 mL of a mixed metal salt solution using carbon dioxide-free deionized water. Forty milliliters of alkali solution was prepared with NaOH. The base solution is added and stirred at low speed for 30 minutes at 37°C under nitrogen. The initial precipitate was centrifuged in a cryo-centrifuge at 12,000 rpm for 10 minutes to obtain an initial precipitate that was washed three times with deionized water until the pH was nearly neutral. The precipitate was washed three times with deionized water (40mL) until the pH was nearly neutral. The suspension was transferred to a PTFE-lined stainless steel autoclave and heated at 100°C for 16h. After cooling, the mixture was enriched by centrifugation at 7600rpm in a freezing centrifuge and after reconstitution with purified water, the mixture was freeze-dried and stored for future use. (Carbon dioxide is removed in advance from the deionized water used in the synthesis process).

The Mg-Al-LDHs suspension was removed from the reactor and the Mg-Al-LDHs suspension was added dropwise to the BSA stock solution (100mg/mL) in a 3:1 ratio. The mixture was stirred at high speed for 30 min at room temperature to ensure the adsorption of BSA on the surface of Mg-Al-LDHs. The resulting dispersion was centrifuged at 12,000rpm for 20min to separate the BSA@LDHs from the unbound BSA. The precipitate was washed twice with deionized water to remove the unbound BSA to obtain the BSA@LDHs nanocarrier. After re-solubilized with deionized water, it was freeze-dried and stored for subsequent experiments.

Resveratrol was dissolved in anhydrous ethanol at a calculated ratio and added dropwise to the synthesized BSA@LDHs and the mixture was stirred in a room temperature water bath for 2 hours under nitrogen atmosphere. The mixture was collected by centrifugation as described above and lyophilized for subsequent experiments.

Characterization

A drop of diluted Mg-Al-LDHs, BSA@LDHs and BSA@LDHs-Res solution was placed on a carbon coated copper TEM grid. The transmission electron microscopy (TEM) images were acquired on JEM-1230 TEM (Hitachi, Japan) at an acceleration voltage of 120 kV. Suspensions of Mg-Al-LDHs powders were prepared by weighing appropriate quantities of Mg-Al-LDHs powders, and after gradient dilution, the particle size distribution and zeta potential were measured using

Malvern Instruments Laser Particle Size Analysis (Malvern, UK). The particle size distribution and zeta potential of the BSA@LDHs and BSA@LDHs-Res samples were determined using the same method. X-ray powder diffraction (XRD) patterns were measured on a Rigaku Miniflex diffractometer (Bruker, Germany) using Cu Kα radiation (λ = 1.54060 Å, 40 kV, 40 mA, in steps of 0.0330°) over a recording range of 5° to 80°.

Fourier transform infrared spectroscopy (FT-IR) (Bruker, Germany) was used to determine the structure and chemical composition of Mg-Al-LDHs, BSA@LDHs and BSA@LDHs-Res nanopreparations. Measurements were performed on a Bruker Vector 22 FT-IR spectrophotometer in the range of 400–4000 cm^{-1}. The UV spectra in the wavelength range of 200–500 nm were determined by measuring the UV absorption of the nanoparticles with a UV spectrophotometer (UV, 3100, Hitachi, Japan). BSA@LDHs-Res powder was weighed into a centrifuge tube, and 8 mL of PBS (pH 5.5, 6.2, 7.4, respectively) was added, and the powder was shaken in a shaker at 37 °C and 100 rpm. 1.5 mL of PBS was taken out at 10, 20, 30, 60, 120, 180, 240, and 360 min, and the absorbance of the powder was measured by UV spectrophotometer. The release rate was calculated by comparing the resveratrol standard curve with the BSA@LDHs-Res loading.

In vitro Cellular Uptake Analysis

Cellular uptake of nanoparticles was tracked using BSA@LDHs-FITC. FITC powder was combined with BSA@LDHs-Res on a shaker, and MDA-MB-231 and SKBR3 cells were inoculated at a density of 1×10^4 into laser confocal Petri dishes, stabilized for 24h and then treated with BSA@LDHs-Res-FITC. The laser confocal dishes were treated with phosphate buffer at different time points (0, 1, 4, 12, 24, 48, 72h) to remove excess particles. Cells were fixed with 4% paraformaldehyde. Cell nuclei were stained with DAPI for 10 min and then washed three times with PBS. The results were observed using a confocal laser scanning microscope (Olympus FV-1200 MPE, Japan).

Lysosomal Escape Experiments

MDA-MB-231 and SKBR3 were localized using BSA@LDHs-Res-FITC. 1×10^4 cells were inoculated in laser confocal dishes and cultured in medium at 37°C for 12 hours. The cells were then incubated with BSA@LDHs-Res-FITC for 3 hours, followed by rinsing twice with cold PBS, then staining the cells with Lysotracker-Red to label lysosomes in the nucleus, and labeling the nucleus with Hoechst 33342, and then observing the results with a laser confocal scanning microscope.

Acridine orange (AO) staining was used to determine the lysosomal membrane permeability: two kinds of cells were inoculated into laser confocal culture dishes, and after the cells were wall-adhered and unfolded, 5μM BSA@LDHs-Res dose solution was added, and the liquid in the dishes was discarded after 24 hours of incubation, and AO staining solution with a final concentration of 10 μg/mL was added in a dark environment, and the cells were left to stand for 15 minutes. Cells were rinsed with PBS, 400μL of 4% paraformaldehyde was added to each dish and fixed for 15 min. Cells were rinsed with PBS, nuclei were stained with Hoechst 33342, and the green (Em=490 nm, Ex=528 nm) and red (Em=555 nm, Ex=617 nm) fluorescence channels were visualized under a laser confocal microscope. The results were observed using a confocal laser scanning microscope (Olympus FV-1200 MPE, Japan).

Cell Proliferation Assay

The effects of different concentrations of BSA@LDHs, Res and BSA@LDHs-Res on the cell viability of SKBR3, MDA-MB-231 and normal mammary cells MCF-10A were detected by CCK-8 method. SKBR3, MDA-MB-231 and MCF-10A cells were uniformly inoculated into 96-well plates at a density of 4×10^3 per well and cultured in 200 μL DMEM medium for 24 hours. Then SKBR3 was cultured in fresh medium (200 μL/well) containing Res (10 μM, 20 μM, 50 μM, 100 μM, 200 μM), BSA@LDHs-Res (10 μM, 20 μM, 50 μM, 100μ M, 200μM) and BSA@LDHs, respectively. MDA-MB-231 was cultured in fresh medium (200 μL/well) containing Res (20 μM, 40 μM, 80 μM, 100 μM), BSA@LDHs-Res (20 μM, 40 μM, 80 μM, 100 μM) and BSA@LDHs. MCF-10A was cultured in fresh medium (200 μL/well) containing Res (10 μM, 20 μM, 30 μM, 400μM), BSA@LDHs-Res (10 μM, 20 μM, 30 μM, 400 μM), and BSA@LDHs, respectively. OD values at 450 nm were measured using a multifunctional enzyme marker (Multiskan GO, Thermo, USA).

Cell Migration and Invasion Assay

SKBR3 and MDA-MB-231 cells were inoculated into six-well plates and cultured until fusion. A single wound tip cut fused monolayer of cells was generated using a 10μL sterile pipette. Cells were rinsed twice with PBS and then incubated with DMEM containing 1% FBS. Cells were treated with BSA@LDHs, Res and BSA@LDHs-Res, and images were recorded at 0h, 24h and 48h, respectively, and the results were observed with an inverted microscope (CKX31, Olympus, Japan).

SKBR3 with MDA-MB-231 cells were seeded at 1×10^5 into six-well plates, and the cells were treated with BSA@LDHs, Res and BSA@LDHs-Res after 24h. After 48h of incubation, cells were digested with trypsin and suspended in serum-free medium. Cells were counted with the same number of cells in each group. The upper chamber of the transwell was inoculated with 200μL of cell suspension, and 700μL of complete medium with 10% FBS was added to the lower chamber of the transwell. 24 hours later, the old medium was aspirated. The transwell was fixed in 4% paraformaldehyde for 30 minutes and then stained with 0.1% Stain Violet solution for 15 minutes at room temperature. In the cell invasion assay, it is necessary to spread a layer of matrix gel on the upper chamber of the transwell cell culture dish in advance, and the rest of the steps are the same as cell migration. The results were observed with an inverted microscope (CKX31, Olympus, Japan).

Cell Apoptosis

The effect of BSA@LDHs-Res nano preparation on the apoptosis of breast cancer cells SKBR3 and MDA-MB-231 was detected by membrane-bound protein V-FITC/PI assay. SKBR3 and MDA-MB-231 were inoculated into six-well plates and cultured for 24 hours per well. The blank group was kept, and the cells of the experimental group were cultured in medium containing BSA@LDHs, Res and BSA@LDHs-Res in a 5% CO2 constant temperature incubator for 48 h. The cells of the experimental group were then incubated with 0.25% of BSA@LDHs, Res and BSA@LDHs-Res in a constant temperature incubator. The cells were then digested with 0.25% trypsin (without EDTA) and collected. After rinsing twice with pre-cooled PBS, 500μL of binding buffer dilution was added. Then, 5μL of membrane-bound protein V-FITC and 5μL of PI were added, and the cells were fully incubated for 15 minutes at room temperature in the dark. Within 1 h, observation and detection were performed using flow cytometry (FACS).

Mitochondrial Membrane Potential Analysis

Mitochondrial membrane potential (MMP) was detected by flow cytometry using JC-1 assay kit. The effect of BSA@LDHs-Res nano preparation on the mitochondrial membrane potential of SKBR3 and MDA-MB-231 cells was investigated. SKBR3 and MDA-MB-231 were inoculated into six-well plates and cultured for 24 hours per well. After resuspending SKBR3 and MDA-MB-231 cells with PBS, the cells of the experimental group were placed in medium containing BSA@s, Res and BSA@LDHs-Res and cultured for 48 hours in a 5% CO_2 incubator. The cells were then digested with 0.25% trypsin and collected. 500μL of cell culture medium and pre-configured JC-1 working solution were added. Cells were then fully incubated in the dark at 37°C for 20 minutes and resuspended using the configured buffer. Within 1 hour, cells were observed and detected using flow cytometry (FACS).

Analysis of Reactive Oxygen Species (ROS) Generation

SKBR3 and MDA-MB-231 cells were inoculated in six-well plates, and after 24h, the medium of the experimental group was changed to a drug solution containing BSA@LDHs, Res and BSA@LDHs-Res. After 48h of incubation, the cells were digested and centrifuged, and then resuspended with a pre-configured DCFH-DA (ROS probe) solution, and then incubated at 37°C for 20 min, and the unbound probe was washed with PBS. Detection was performed using flow cytometry within 1h.

Glucose Consumption and Lactate Measurement

SKBR3 and MDA-MB-231 cells were inoculated into six-well plates at 1×10^5 and cultured for 24h. After that, the cells were treated with drug solutions added with BSA@LDHs, Res, and BSA@LDHs-Res, respectively, and the medium was

exchanged for FBS-free medium, and the supernatants were collected. Glucose consumption and lactate release were measured using glucose and lactate kits.

Lactate Dehydrogenase and ATP Measurements

SKBR3 and MDA-MB-231 cells were inoculated at 1×10^5 into six-well plates and cultured for 24h. After that, the cells were treated with drug solutions supplemented with BSA@LDHs, Res and BSA@LDHs-Res, respectively. After 48 hours of incubation, the cells were treated with lactate dehydrogenase viability assay kit and ATP assay kit protocols and assayed using a multifunctional enzyme marker.

Western Blot Assay

SKBR3 and MDA-MB-231 cells in logarithmic growth phase were inoculated into 6-well plates at a density of 4×10^5 cells/well and cultured for 24h. After 24h of incubation, 2mL of medium containing the same concentration of BSA@LDHs, Res and BSA@LDHs-Res were added. After 24h of treatment, cells of each group were collected and protein extracts were prepared in the ratio of 1mLRIPA to 10μL PMSF. Protein content was quantified by BCA protein quantification. Protein samples were separated by SDS-PAGE gel electrophoresis, transferred to polyvinylidene difluoride (PVDF) membranes, closed with a sealing solution and incubated with primary and secondary antibodies. Finally, the expression of GLUT1, PKM2 and HK2 proteins in each group was observed on a gel imager (ChemiDoc^{TM}XRS+, Bio-Rad, USA).

Treatment of Tumor-Bearing Mice

A xenograft tumor model was established by subcutaneous injection of 5×10^5 SKBR3 cells/80μL of saline into the right abdomen of mice. The tumor model was established one week later when the tumor had grown to a volume of approximately 60 cubic millimetres. The mice were grouped as follows: control group, BSA@LDHs group, Res group and BSA@LDHs-Res group. Peritumoral injections of PBS containing BSA@LDHs-Res, Res, BSA@LDH, and PBS (n = 6) were assigned the appropriate material concentration based on the injection of standard Res at a concentration of 20 mg/kg. The frequency of injections was once every 2 days for 12 consecutive days and body weight and tumor volume were recorded. Tumor volume was calculated as: tumor volume (mm^3) = 0.5 × (length × width × width).

H&E Staining, Immunohistochemistry and TUNEL Staining

At the end of the experiment, tumors, hearts, livers, spleens, lungs and kidneys from each group were collected, and tumor tissues and major organs were fixed using 4% paraformaldehyde and embedded in paraffin. Apoptosis was measured using the TUNEL Apoptosis Detection Kit, which was cut into 5 μm-thick sections, and each section was injected with a drop of 50μL of the assay solution and incubated for 60 minutes at 37°C. The samples were then incubated with PBS and washed with PBS. Sections were washed with PBS, treated with Triton X-100 for 10 minutes at room temperature, and the nuclei were counterstained with DAPI before sealing with 5% bovine serum albumin. Tumor tissues and major organs of mice were deparaffinized in xylene and routinely stained with hematoxylin-Iranian hematoxylin and eosin (H&E) for routine histopathological analysis. IHC was performed using Ki67 antibody immunohistochemistry kit. Immunofluorescence using GLUT1 and PKM2 antibodies. Tumor tissues were stained using the corresponding antibodies, incubated overnight at 4°C, washed and incubated with secondary antibody (red fluorescent) for 2 h. Tumor tissues were restained with DAPI, washed and sealed with glycerol. All images were taken under a microscope (Eclipse C1, Nikon, Japan).

Statistical Analysis

All data are expressed as the mean ± standard deviation (SD). The *t*-test was used to compare differences between two groups, while one-way ANOVA was employed to analyze differences among three or more groups. Statistical analyses were conducted using GraphPad Prism 9.0 software. Significance is denoted as *$p < 0.05$, **$p < 0.01$, and ***$p < 0.001$.

Results

Preparation and Characterization of BSA@LDHs and BSA@LDHs-Res

The results of our study confirm the successful preparation of both BSA@LDHs and BSA@LDHs-Res nanocarrier systems. We began by preparing Mg-Al-LDHs, BSA@LDHs, and BSA@LDHs-Res using hydrothermal co-precipitation, as illustrated in Figure 1A. The LDHs carriers were observed to have typical hexagonal lamellar structures with clear contours and dispersion boundaries, as shown in Figure 1B. The incorporation of resveratrol led to a transition in nanoparticle morphology from a regular hexagonal shape to a more irregular one, yet the lamellar structure remained discernible. The average particle sizes, measured

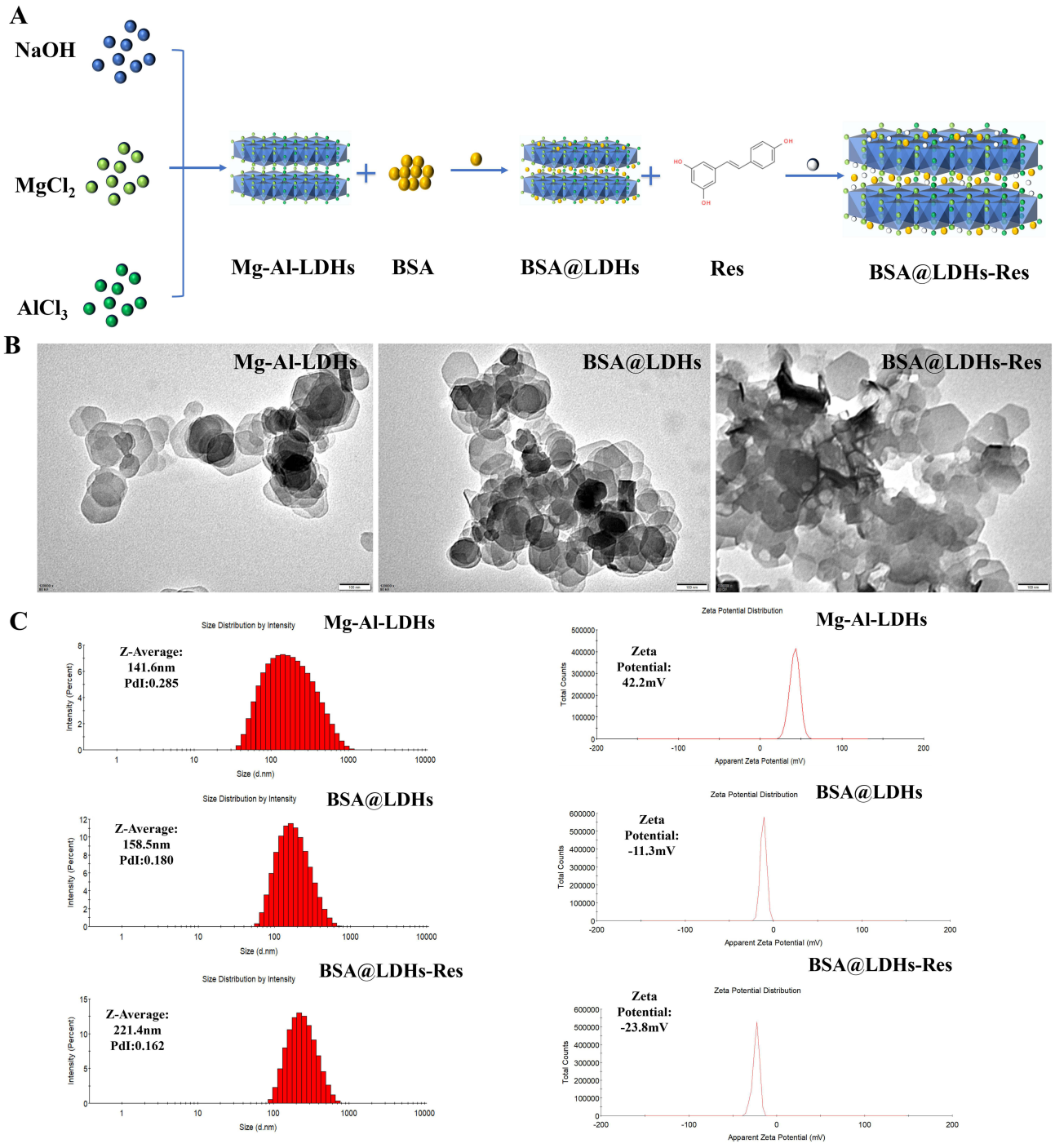

Figure 1 Continued.

https://doi.org/10.2147/IJN.S492145

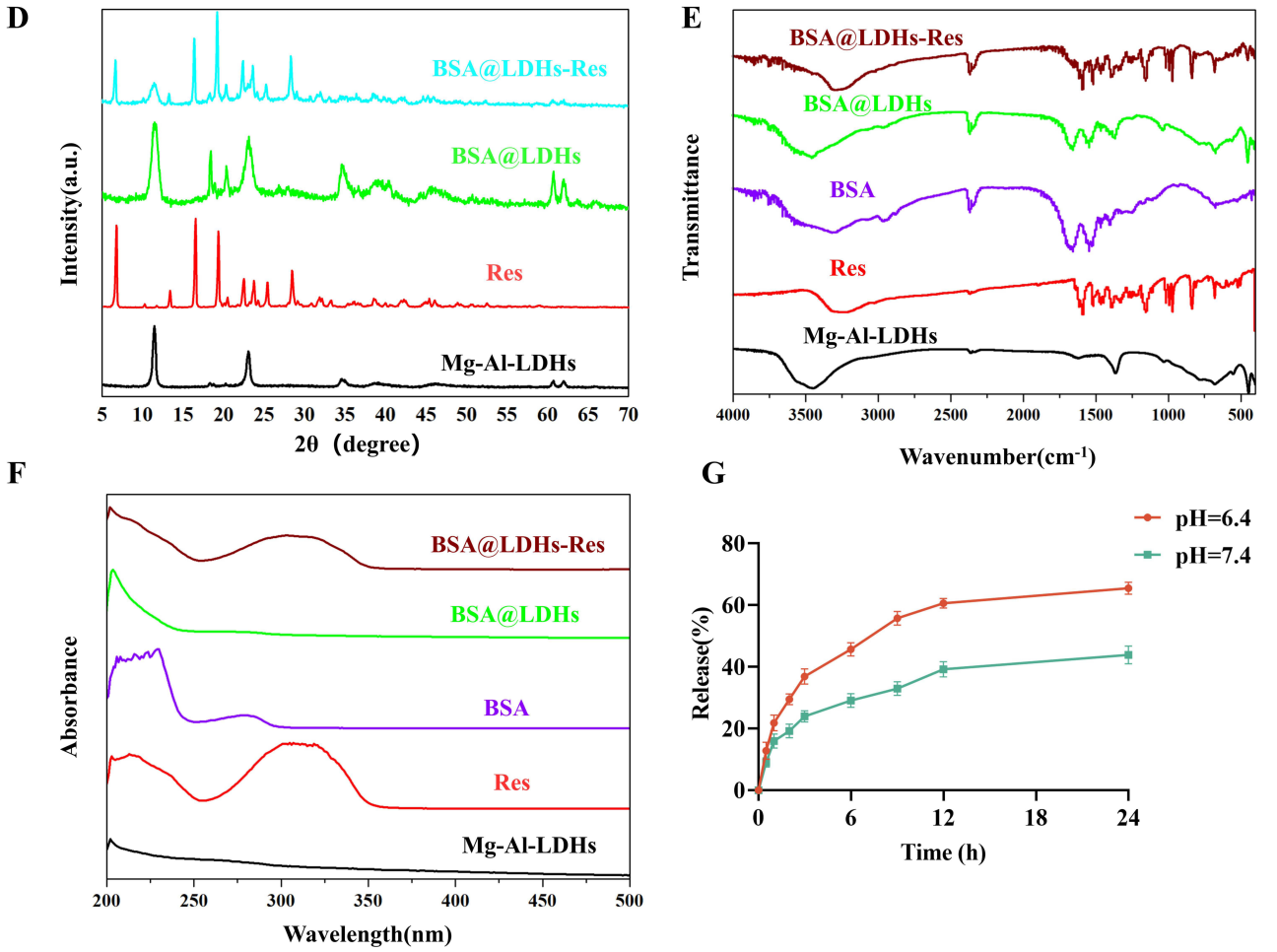

Figure 1 (**A**) Schematic of the synthesis routes of Mg-Al-LDHs, BSA@LDHs and BSA@LDHs-Res (**B**) TEM images of Mg-Al-LDHs, BSA@LDHs, Res and BSA@LDHs-Res at 100 nm size. (**C**) Particle size distribution of Mg-Al-LDHs, BSA@LDHs, Res, and BSA@LDHs-Res, with PDI representing polymer dispersion index; Zeta potentials of Mg-Al-LDHs, BSA@LDHs, Res, and BSA@LDHs-Res; (**D**) XRD spectra of Mg-Al-LDHs, Res, BSA, BSA@LDHs, BSA@LDHs-Res; (**E**) FTIR spectra of Mg-Al-LDHs, Res, BSA, BSA@LDHs, BSA@LDHs-Res; (**F**) UV spectra of Mg-Al-LDHs, Res, BSA, BSA@LDHs, BSA@LDHs-Res.(**G**) Drug release curves of BSA@LDHs-Res in phosphate buffers at pH=6.4 and 7.4.

using dynamic light scattering (DLS), were found to be 141.6± 2.4 nm for Mg-Al-LDHs, 158.5± 3.0 nm for BSA@LDHs, and 221.4 ± 1.8 nm for BSA@LDHs-Res, as detailed in Figure 1C.

The zeta potential measurements provided further insights into the surface charge of the nanoparticles. The mean zeta potentials of Mg-Al-LDHs, BSA@LDHs, and BSA@LDHs-Res were determined to be +42.2± 1.6 mV, −11.3 ±1.0 mV, and −23.8 ± 1.4 mV, respectively. This shift from a positive to a negative zeta potential upon the addition of BSA and Res is attributed to the interactions between the albumin and the drug, which modulate the potential of the nanocarrier system. Notably, BSA@LDHs-Res nanoparticles demonstrated enhanced stability with a zeta potential of −23 mV, indicating a repulsive force between particles that contributes to the overall system stability.

The crystalline structure of the materials was further assessed through diffraction peak analysis presented in Figure 1D. These peaks confirmed the stability of the crystal structure, and a comparison across the four spectra revealed that all visible diffraction peaks were consistent with the original Mg-Al-LDHs sample. This consistency suggests that the addition of resveratrol molecules or BSA proteins did not result in the formation of new crystal phases.

To further investigate the interactions between the components, we examined the FTIR spectra, as shown in Figure 1E. A shift to the left in the first characteristic peak of BSA@LDHs-Res, attributed to OH bonding, indicates the formation of interactions between LDHs and BSA, confirming the absorption of BSA by the nanoparticles. The

presence of characteristic peaks for LDHs, BSA, and Res in both BSA@LDHs and BSA@LDHs-Res, without any new peaks, suggests that BSA and Res were successfully loaded into LDHs and physically bound.

Finally, the UV-visible spectra in Figure 1F correspond to the maximum absorption wavelengths of LDHs, BSA, and Res, indicating that BSA and Res were successfully loaded and chemically bound into LDHs. To assess the drug release profile, we studied the percentage of drug release in both acidic (pH = 6.4, simulating the tumor microenvironment) and neutral (pH = 7.4, simulating physiological conditions) environments. Over a 24-hour period, only 43.69% of the drug was released at pH = 7.4, but this percentage increased to 65.24% at pH = 6.4. This increase in drug release at acidic pH suggests that the tumor microenvironment may play a role in facilitating drug release, which is a desirable characteristic for targeted cancer therapy (Figure 1G).

Analysis of Drug Loading and Cell Uptake Analysis

We obtained the UV full-wavelength scanning curve of Res and observed its maximum absorption peak at 306 nm. As shown in Figure 2A, both MDA-MB-231 and SKBR-3 cells began to absorb the aspirated BSA@LDHs-Res nano-loaded particles within an hour. Over time, the amount of nanodrugs ingested by the cells increased, while the intensity of green fluorescence decreased, indicating drug depletion. However, after 72 hours, MDA-MB-231 and SKBR-3 cells exhibited only trace fluorescence, suggesting that BSA@LDHs-Res maintains its effectiveness over an extended period. Furthermore, we investigated the distribution of BSA@LDHs within MDA-MB-231 and SKBR3 breast cancer cells.

The lysosomal red fluorescent probe Lysotracker Red, known for its ability to pass through cell membranes and stain lysosomes in living cells, was used to track the fate of BSA@LDHs-Res within MDA-MB-231 and SKBR3 cells. Figure 2B illustrates that upon the absorption of BSA@LDHs-Res by these cells, there was a noticeable overlap between the red fluorescence of the lysosomes and the green fluorescence of BSA@LDHs-Res. This co-localization suggests that while the nanocarrier system is internalized, it may avoid lysosomal capture, which is a common pathway for the degradation of internalized substances.

Acridine orange (AO), a fluorescent dye that changes color based on its environment, was also employed to assess lysosomal function. AO emits red fluorescence in lysosomes and green-red fluorescence in the cytoplasm. Figure 2C shows that control MDA-MB-231 and SKBR3 cells exhibited strong red fluorescence, indicating active lysosomes. However, cells treated with BSA@LDHs-Res displayed weaker red fluorescence and stronger green fluorescence, suggesting an increase in lysosomal membrane permeability. This permeability change allows AO to leak from the lysosomes into the cytoplasm, indicating a disruption in the normal lysosomal function.

These experimental results point to the lysosomal escape mechanism of BSA@LDHs-Res. By evading the lysosomal pathway, BSA@LDHs-Res reduces the risk of drug clearance by intracellular lysosomes. This evasion strategy not only increases the drug delivery efficiency but also prolongs the drug's action duration within the cells. Consequently, the BSA@LDHs-Res nanocarrier system plays a crucial role in maintaining the efficient and stable function of Res in breast cancer cells MDA-MB-231 and SKBR3, as supported by the data presented. This system's ability to bypass lysosomal degradation is a significant factor in its sustained efficacy against breast cancer cells.

Inhibition of Migration and Invasion by BSA@LDHs-Res

In our study, we utilized the CCK-8 assay to assess the inhibitory effects of varying concentrations of free Res and BSA@LDHs-Res on the proliferation of breast cancer cells SKBR3 and MDA-MB-231 over a 48-hour period. Figure 3A demonstrated that after 48 hours of treatment with different concentrations of Res and BSA@LDHs-Res, there were significant differences in the inhibition of cell growth in SKBR3 and MDA-MB-231 cells. Specifically, treatment with 20 μmol/L or 35 μmol/L of BSA@LDHs did not induce significant toxicity in these breast cancer cells. However, SKBR3 cells exhibited dose-dependent cytotoxicity when treated with BSA@LDHs-Res at concentrations ranging from 10 μmol/L to 200 μmol/L, which was significantly different from the cytotoxicity observed in cells treated with equivalent concentrations of free Res. As the concentration increased from 10 μmol/L to 100 μmol/L, the cytotoxicity in MDA-MB-231 cells treated with BSA@LDHs-Res markedly increased compared to those treated with the same concentration of free Res.

Furthermore, we assessed the impact of various concentrations of BSA@LDHs, Res, and BSA@LDHs-Res on normal mammary epithelial cells MCF-10A and found no significant effects. At low concentrations, we observed

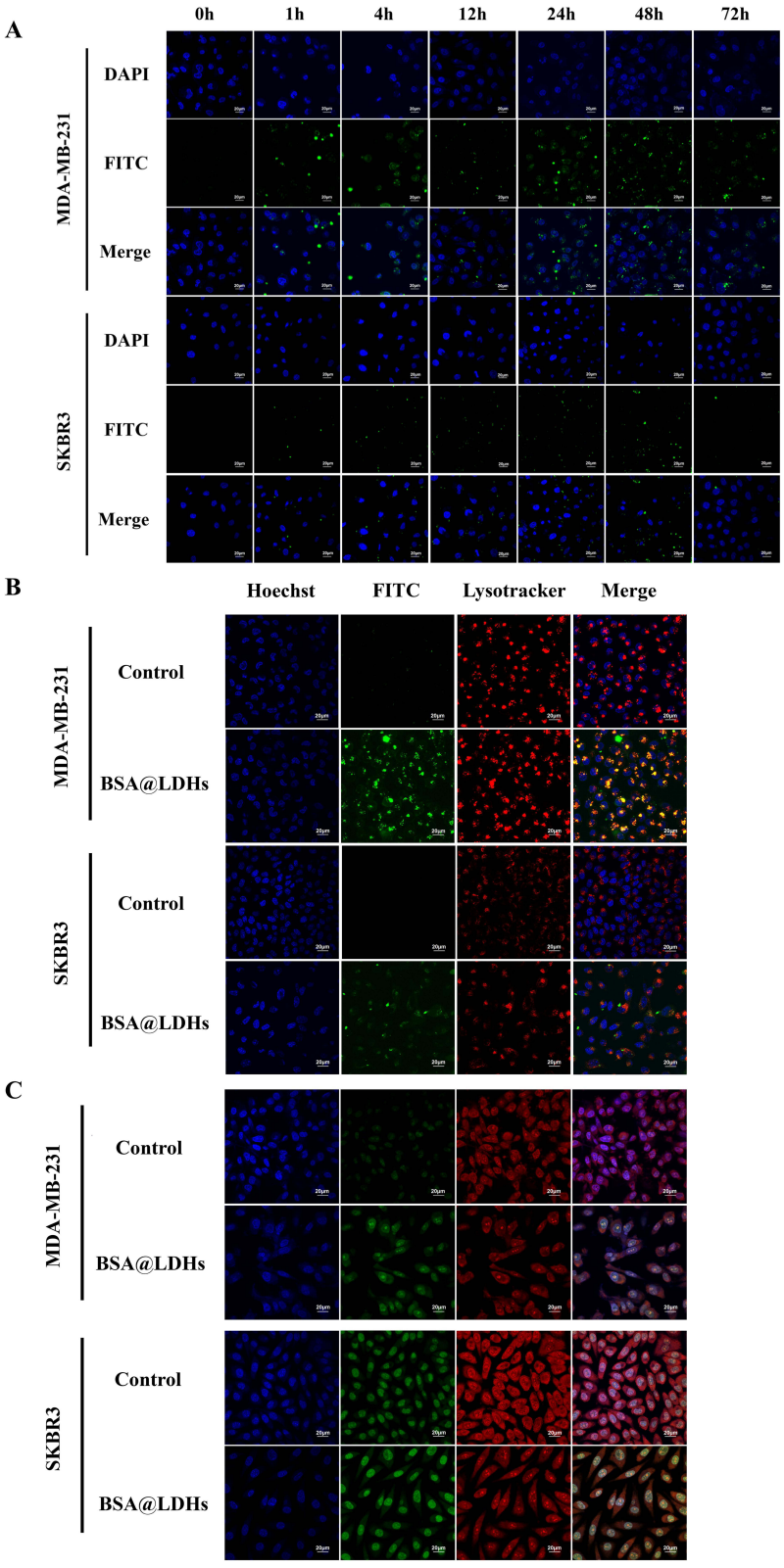

Figure 2 (**A**) Confocal images of MDA-MB-231 and SKBR3 cells at different time points of BSA@LDHs-Res (FITC) and nuclei (DAPI), scale bar: 20μm; (**B**) Localisation of BSA@LDHs-Res (FITC) in MDA-MB-231 and SKBR3 cells after 48 h of drug treatment with BSA@LDHs-Res and labelled with Hoechst 33342 (blue) and Lysotracker-red (red) to differentiate between nuclei and lysosomes, respectively, scale bar: 20μm; (**C**) Acridine Orange staining to detect lysosomal membrane permeability, red fluorescence versus green fluorescence to reflect the size of lysosomal membrane permeability, and labelling of nuclei of both cells with Hoechst 33342 (blue), scale bar: 20μm.

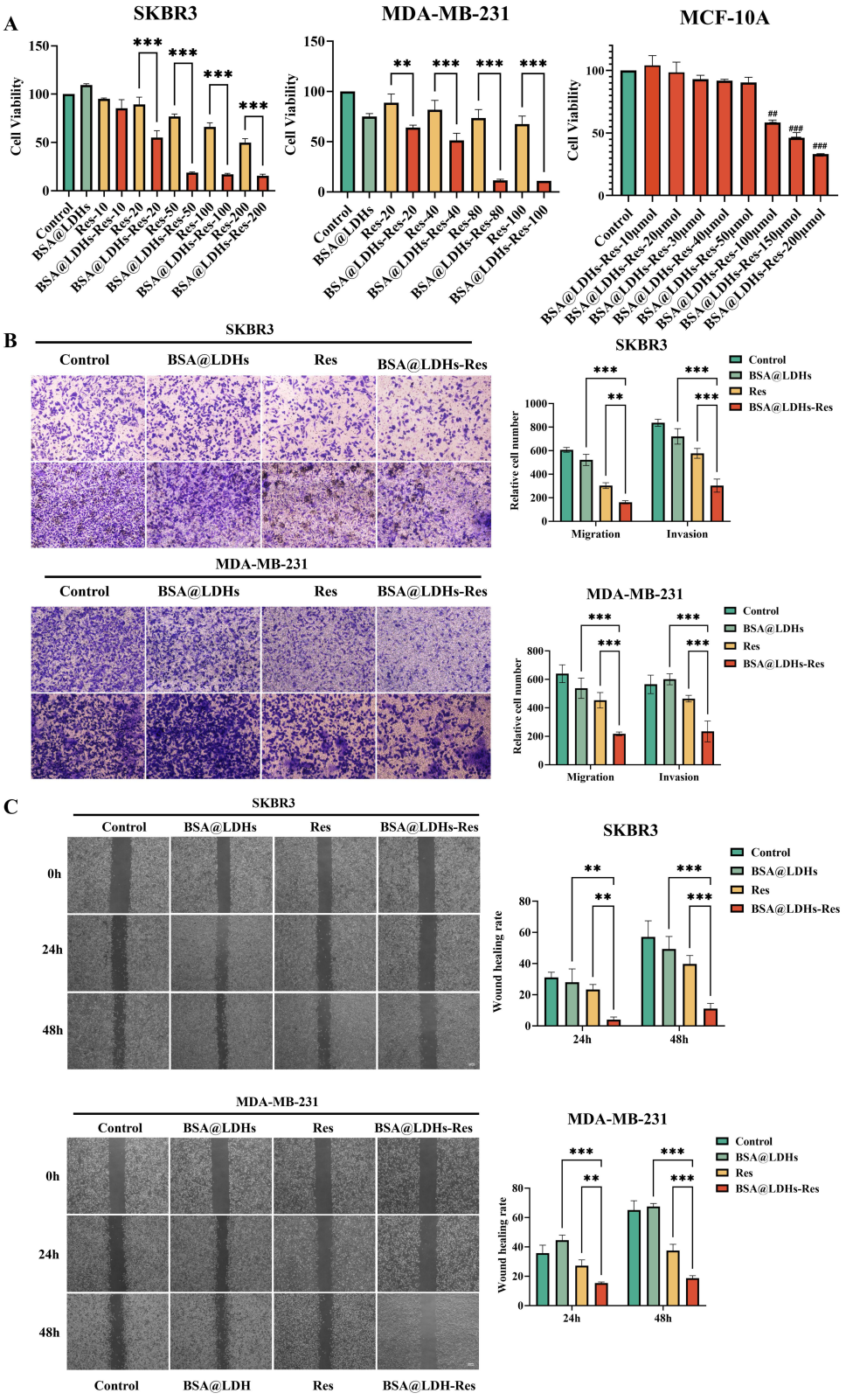

Figure 3 (**A**)Comparison of SKBR3, MDA-MB-231 and MCF-10A cell survival after 48 h treatment with BSA@LDHs, different concentrations of Res and BSA@LDHs-Res. (**B**) Transmembrane number of cells was detected using the migration and invasion assay. Representative micrographs of SKBR3 cells and MDA-MB-231 cells in the Boyden chamber. Scale bar: 200μm; (**C**) Wound healing assay was used to assess cell migration. Wound healing images of cells treated with BSA@LDHs, Res and BSA@LDHs-Res for 0, 24 and 48 h and untreated. Scale bar: 200μm. Scale bar: 200μm. Data are expressed as mean ± SD (n=3), **P < 0.01, ***P < 0.001. # stands for statistics with Control, $^{\#\#}$P < 0.01, $^{\#\#\#}$P < 0.001.

https://doi.org/10.2147/IJN.S492145

some value-adding effects, indicating that both BSA@LDHs and BSA@LDHs-Res were biologically safe. Consequently, for subsequent experiments, we selected 20 μmol/L of BSA@LDHs-Res, Res, and BSA@LDHs, along with a blank control group, for the treatment of SKBR3 cells. Similarly, a concentration of 30 μmol/L was chosen for the treatment of MDA-MB-231 cells. These concentrations were chosen to ensure a comprehensive comparison of the effects of free Res and the nanocarrier system on breast cancer cell proliferation.

We also employed the wound healing, transwell migration, and invasion assays to assess the impact of BSA@LDHs-Res on the migration and invasion of SKBR3 and MDA-MB-231 cells. Our findings from the scratch assay, as well as the transwell migration and invasion assays, revealed that both the Res and BSA@LDHs-Res groups exhibited reduced cell migration capacity compared to the control group. Notably, the BSA@LDHs-Res group demonstrated a significantly lower cell migration rate than the Res group alone. As depicted in Figure 3B, the number of cells that migrated and invaded through the chambers in the transwell assays was significantly lower in the Res and BSA@LDHs-Res groups than in the control group. Furthermore, the presence of BSA@LDHs-Res significantly impeded the movement and invasion of SKBR3 and MDA-MB-231 cells more than Res treatment alone. Figure 3C illustrates that while the control group had superior wound healing compared to both the Res and BSA@LDHs-Res groups, the BSA@LDHs-Res group showed improved wound healing inhibition in SKBR3 and MDA-MB-231 cells compared to the group treated with Res alone. These results suggested that BSA@LDHs-Res effectively suppressed the migratory and invasive capabilities of breast cancer cells.

Glycolysis Level Analysis

Normal cells maintain glucose homeostasis by converting glucose into pyruvate and lactate under hypoxic conditions, and they enter the tricarboxylic acid (TCA) cycle when oxygen levels are sufficient.[18] In contrast, cancer cells undergo aerobic glycolysis, a process in which they convert glucose to lactate from pyruvate and generate ATP, even in the presence of oxygen.[19] This metabolic pathway leads to an increased uptake of glucose and lactate in tumor cells, alongside elevated ATP production through glycolysis, which in turn promotes tumor growth.[20] Key glycolytic enzymes become more active as aerobic glycolysis increases.

Our study demonstrated a significant reduction in lactate accumulation and glucose uptake in MDA-MB-231 and SKBR3 cells treated with BSA@LDHs-Res, as shown in Figures 4A, andFigures 4B suggesting a disruption in their internal glycolytic processes. Lactate dehydrogenase, a crucial enzyme in glycolysis, showed a marked decrease in activity when BSA@LDHs-Res was introduced to MDA-MB-231 and SKBR3 cells, as illustrated in Figure 4C. Post-treatment, these cells exhibited a loss of glycolytic capacity, leading to a diminished ATP production from glycolysis. Figure 4D clearly shows the substantial decrease in ATP levels within BSA@LDHs-Res-treated MDA-MB-231 and SKBR3 cells. This decrease in ATP production is a critical finding, as it indicates that BSA@LDHs-Res treatment impairs the energy metabolism of breast cancer cells, thereby inhibiting their growth and survival.

Effects of BSA@LDHs-Res on Apoptosis, Reactive Oxygen Species (ROS) Generation and Mitochondrial Membrane Potential (MMP)

Mitochondria are pivotal organelles in breast cancer cells, playing a critical role in the apoptotic pathway. Apoptosis is characterized by a decrease in ATP and mitochondrial membrane potential (MMP), and an increase in reactive oxygen species (ROS) levels is indicative of mitochondrial dysfunction.[19] Our study aimed to investigate how the modulation of glycolysis by the BSA@LDHs-Res nanocarrier system affected these mitochondrial functions and, consequently, influenced apoptosis in SKBR3 and MDA-MB-231 cells.

Figure 5A demonstrated that treating these cells with Res and BSA@LDHs-Res for 48 hours led to a significant increase in apoptosis rates, with BSA@LDHs-Res showing a more pronounced effect at concentrations of 20 μM for SKBR3 and 30 μM for MDA-MB-231 cells. This suggested that the nanocarrier system not only delivered Res effectively but also enhanced its apoptotic potential. The impact of BSA@LDHs-Res on mitochondrial membrane potential was further detailed in Figure 5B. After 48 hours of treatment, significant changes in MMP were observed, indicating that BSA@LDHs-Res disrupted the mitochondrial function in these cells. This disruption in MMP could increase mitochondrial permeability, leading to the

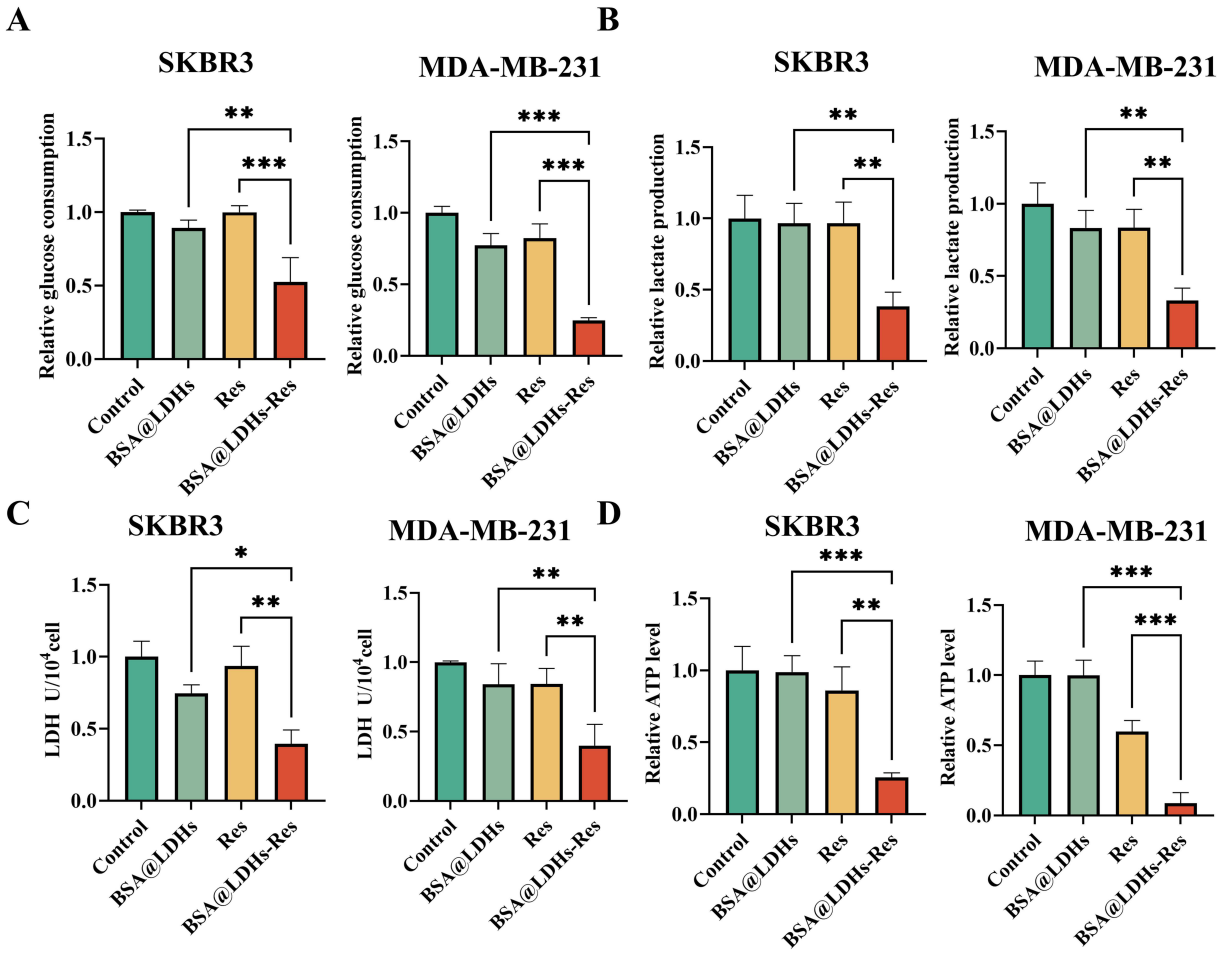

Figure 4 (**A**) Glucose uptake level of SKBR3 and MDA-MB-231 cells after 48 hours of drug treatment; (**B**) Lactate production level of SKBR3 and MDA-MB-231 cells after 48 hours of drug treatment; (**C**) Lactate dehydrogenase level of SKBR3 and MDA-MB-231 cells after 48 hours of drug treatment; (**D**) ATP levels in SKBR3 and MDA-MB-231 cells after 48 hours of drug treatment; data are expressed as mean ± SD (n=3), *P < 0.05, **P < 0.01, ***P < 0.001.

release of pro-apoptotic factors and the initiation of the apoptotic cascade. Figure 5C further supported our hypothesis by showing a significant increase in ROS production in BSA@LDHs-Res-treated cells compared to other groups. This increase in ROS was particularly noteworthy as it indicated a higher delivery efficiency of Res when complexed with BSA@LDHs-Res, as opposed to free Res. The relatively low ROS production in cells treated with free Res, especially at low concentrations, underscored the enhanced efficacy of the nanocarrier system.

In conclusion, the disruption of glycolysis by BSA@LDHs-Res in MDA-MB-231 and SKBR3 cells resulted in a cascade of events: a significant increase in apoptosis, alterations in mitochondrial membrane potential, and an elevation in aggregated ROS levels. These findings suggested that the BSA@LDHs-Res nanocarrier system, by modulating glycolysis and targeting mitochondrial function, effectively induced apoptosis in breast cancer cells. This systematic approach highlighted the potential of BSA@LDHs-Res as a therapeutic agent capable of perturbing the metabolic landscape of cancer cells, thereby promoting their demise.

In vitro Anti-Tumor Mechanism of BSA@LDHs-Res

In the glycolytic pathway, there are three pivotal enzymes that govern aerobic glycolysis: hexokinase (HK2), phosphofructokinase 1 (PFK1), and pyruvate kinase M2 (PKM2). Each of these enzymes is associated with the progression of breast cancer.[21] After administering the drug treatment, we assessed the expression of these key glycolytic enzymes (HK2, PKM2) and the glucose transporter protein GLUT1 in SKBR3 and MDA-MB-231 cells. Figure 6 illustrates that when BSA@LDHs-Res was introduced to SKBR3 and MDA-MB-231 cells, the levels of GLUT1 and the glycolytic key

https://doi.org/10.2147/IJN.S492145

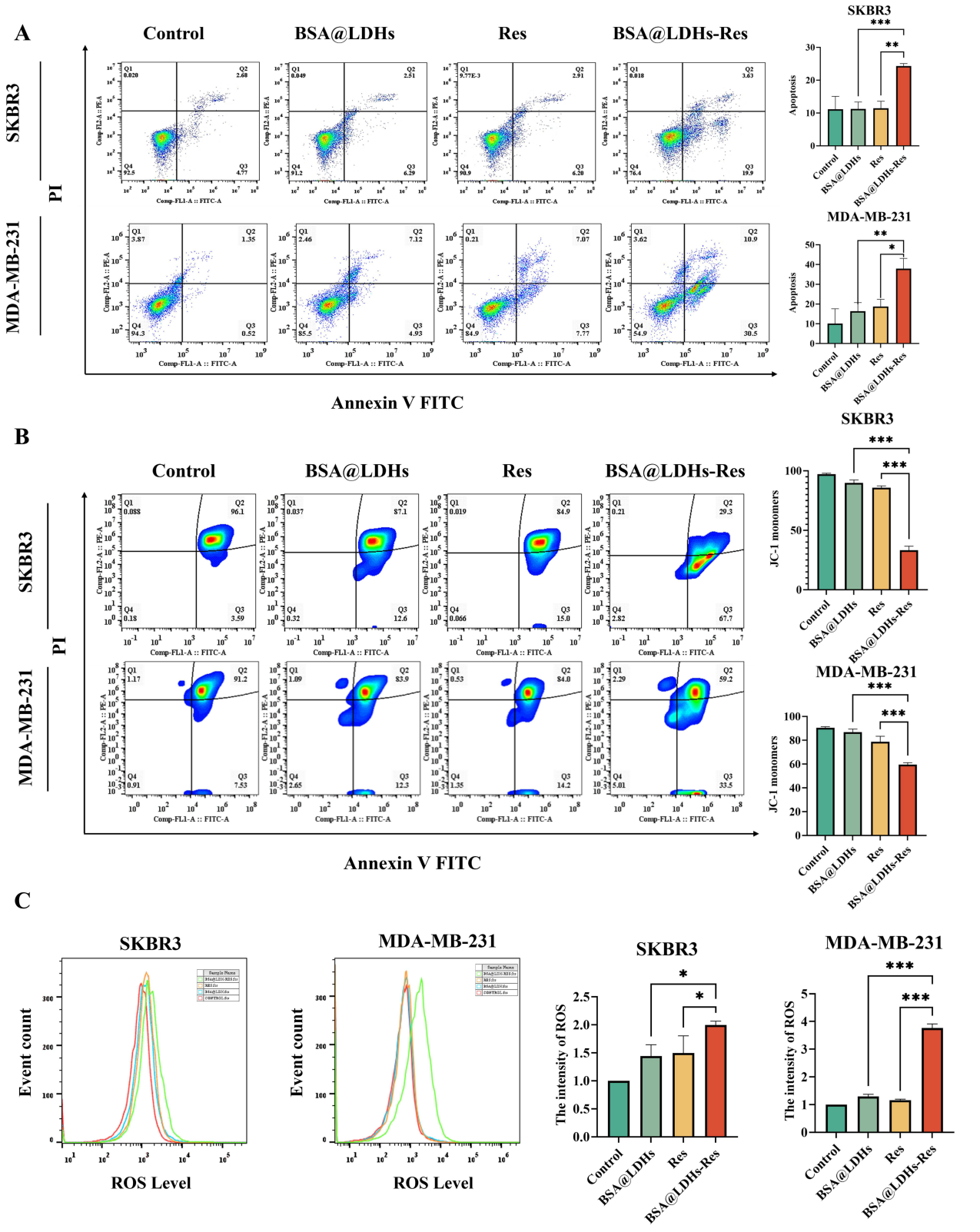

Figure 5 (**A**) Representative images of SKBR3 and MDA-MB-231 cell apoptosis after 48 hours of drug treatment by flow cytometry; (**B**) Representative images of mitochondrial membrane potential changes in SKBR3 and MDA-MB-231 cells in each group after drug treatment detected by flow cytometry; (**C**) ROS levels of SKBR3 and MDA-MB-231 cells in each group after drug treatment by flow cytometry; data are expressed as mean ± SD (n=3), *P < 0.05, **P < 0.01, ***P < 0.001.

https://doi.org/10.2147/IJN.S492145

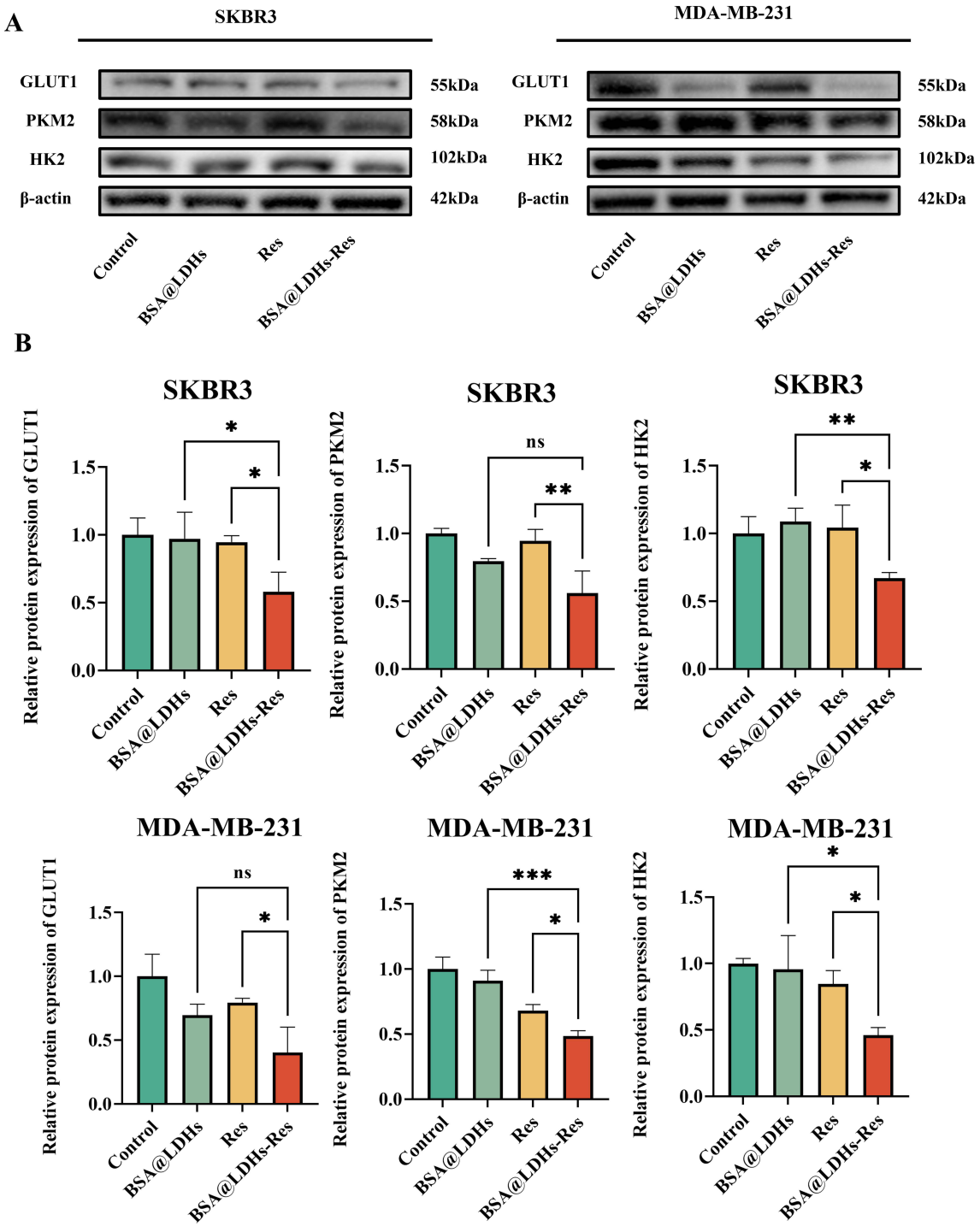

Figure 6 (**A**) Protein expression and quantification of GLUT1, HK2, PKM2 in MDA-MB-231 and SKBR3 cells treated with control, BSA@LDHs, Res, and BSA@LDHs-Res; (**B**) Schematic diagram of the mechanism of cellular glycolysis regulated by BSA@LDHs-Res. Data are expressed as mean ± SD (n=3), *P < 0.05, **P < 0.01, ***P < 0.001.

enzymes HK2 and PKM2 were significantly reduced compared to the Res group. As a result, BSA@LDHs-Res effectively inhibited glycolysis in MDA-MB-231 and SKBR3 breast cancer cells by suppressing GLUT1 and constraining the activity of key glycolytic enzymes.

https://doi.org/10.2147/IJN.S492145

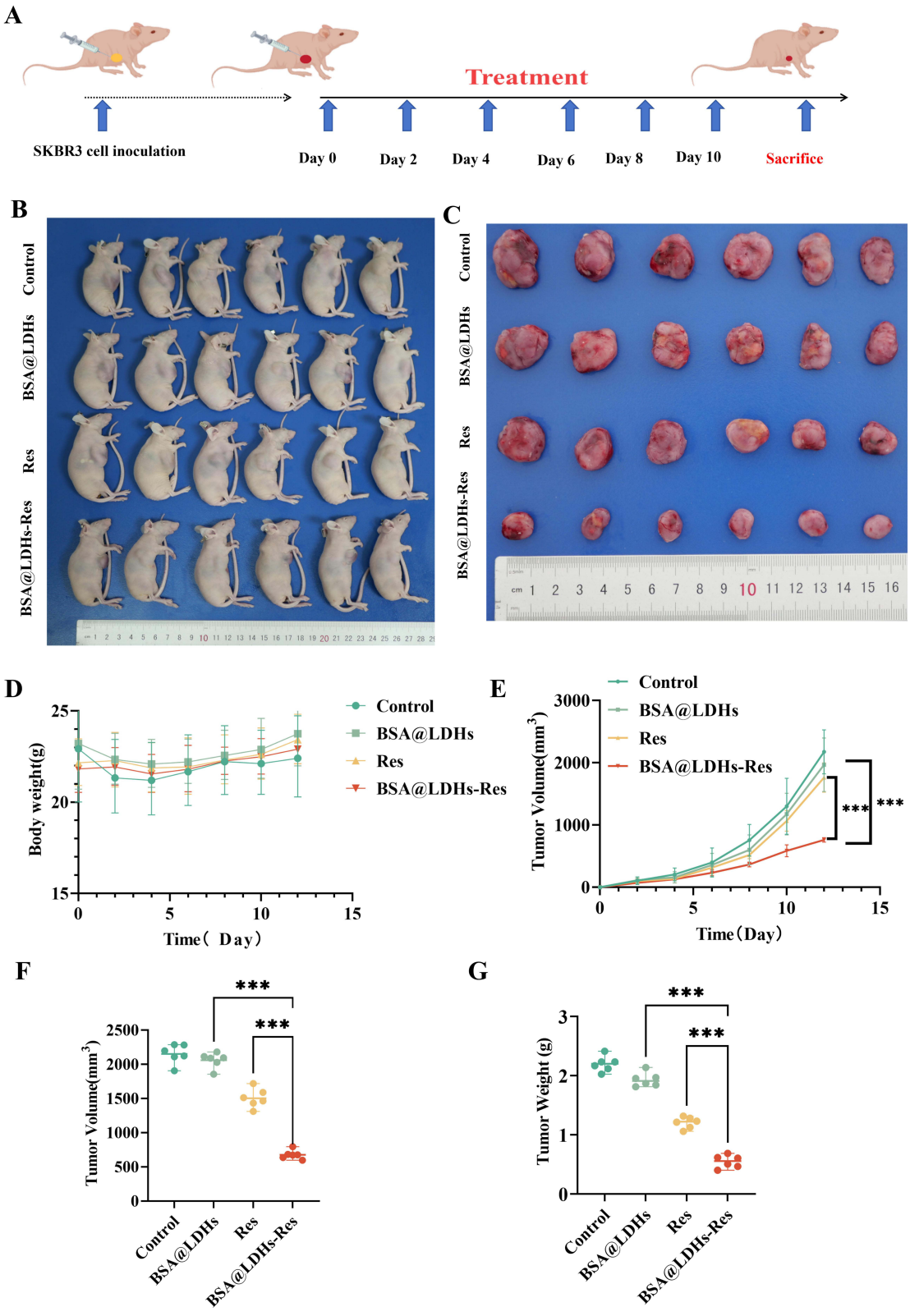

Figure 7 (**A**) Flow chart of BSA@LDHs-Res in vivo treatment of transplanted tumors; (**B**) Tumor growth status after treatment in each treatment group; (**C**) Digital photographs of tumor dissections in each treatment group; (**D**) Curves of body weight over time in different nude mice treatment groups; (**E**) Curves of tumor volume over time in different treatment groups; (**F**) Tumor volumes after dissection of mice in each group; (**G**) Tumor weight of mice in each group after dissection. Data were expressed as mean ± standard deviation (mean ± SD) of 6 mice in each group (n=6). ***p < 0.001.

https://doi.org/10.2147/IJN.S492145

Therapeutic Effect in vivo

In our investigation, we developed a nude mouse tumor model utilizing SKBR3 breast cancer cells, which served as a foundation for evaluating the therapeutic effects of different treatments (as illustrated in Figure 7A). The model was methodically divided into four distinct groups to isolate the effects of various interventions: the PBS group, the BSA@LDHs group, the free Res group, and the BSA@LDHs-Res group. We chose an injection concentration of 20 mg/kg for Res based on established standards, prepared the appropriate material concentrations, and administered PBS containing BSA@LDHs-Res, BSA@LDHs, Res, and PBS peritumorally to each group (n = 6). This peritumoral injection treatment commenced when the tumors reached approximately 80 mm^3, and the mice were subsequently monitored for changes in body weight and tumor volume every two days until the study's endpoint on day 12, as shown in Figure 7B. Figure 7D demonstrated that there was no significant variation in body weight across the different treatment groups, which suggested that the nanomedicine-loaded system we used possessed low toxicity and was biosafe. This finding was crucial, as it indicated that the treatments did not adversely affect the mice's overall health. Figure 7E revealed that the tumor volume in the BSA@LDHs group remained unchanged compared to the PBS group, indicating a lack of therapeutic effect. In contrast, the free Res group showed some inhibitory effect on tumor growth, but it was the BSA@LDHs-Res group that exhibited a significantly reduced tumor volume and lighter tumor weight compared to the other groups. This result pointed to the enhanced efficacy of BSA@LDHs-Res in not only reducing tumor growth but also in shrinking the size of the tumors, highlighting its potential as an effective anti-tumor agent. The photographs of the tumors, along with the corresponding tumor volumes and weights, presented in Figure 7C, D, F, and G, visually corroborated the therapeutic benefits of BSA@LDHs-Res. These visual representations provided a comprehensive view of the tumor's response to treatment, underscoring the efficacy of BSA@LDHs-Res in inhibiting tumor growth and progression. The logical progression from the establishment of the tumor model to the systematic evaluation of treatment effects, and finally to the visualization of tumor response, collectively supported the conclusion that BSA@LDHs-Res is a promising candidate for the treatment of SKBR3 breast cancer.

To further confirm the therapeutic efficacy of the BSA@LDHs-Res nano-loading system, we conducted a comprehensive histological analysis to assess its anti-tumor effects. The H&E staining results revealed a notable presence of pink-stained tumor cells in the BSA@LDHs-Res group compared to other treatment groups, indicating that BSA@LDHs-Res effectively disrupted tumor tissues. In the Ki67 assay, a marker of cellular proliferation, the BSA@LDHs-Res group exhibited the lowest positive rate of brownish-yellow signals, suggesting that BSA@LDHs-Res significantly inhibited tumor cell proliferation. The TUNEL assay, used to detect apoptotic cells, demonstrated that the apoptosis rate in mouse tissues from the BSA@LDHs-Res group was markedly higher than in other treatment groups (as shown in Figure 8A). Immunofluorescence analysis was performed to assess the expression of GLUT1 and PKM2 in tumor tissues, key players in tumor metabolism. The results indicated that the expression levels of GLUT1 and PKM2 in the BSA@LDHs-Res treatment group were significantly lower than those in the free Res treatment group, aligning with our previous cellular level findings (as depicted in Figure 8B). This further confirmed that BSA@LDHs-Res could suppress the metabolic pathways critical for tumor growth. Finally, to evaluate the biocompatibility of BSA@LDHs-Res, we performed H&E staining on heart, liver, spleen, lung, and kidney tissues from nude mice across different treatment groups. Figure 8C illustrates that both BSA@LDHs and BSA@LDHs-Res did not induce any apparent damage to these organs, indicating that BSA@LDHs-Res possesses good biocompatibility and has promising potential in cancer therapy. These collective findings from histological assessments underscore the therapeutic potential of BSA@LDHs-Res as a nano-loading system for cancer treatment, highlighting its ability to target tumor tissues with minimal off-target effects on normal organs.

Discussion

Breast cancer ranks second in incidence and has become the most common type of cancer among women worldwide.[20] Its metastatic and recurrent nature has led to an increasingly challenging form of treatment for breast cancer, with an urgent need to develop new safe and efficient oncology therapies. Breast cancer cells differ significantly from normal breast cells in energy metabolism, and breast cancer cells tend to obtain energy through the glycolytic pathway, which enhances the glycolytic effect aerobic glycolysis even in the presence of sufficient oxygen. It has been shown that the enhanced glycolysis in breast cancer cells is mainly due to the enhanced activity of glycolysis-related enzymes and regulatory factors, and these include pyruvate kinase, hexokinase, phosphofructokinase, lactate dehydrogenase, and

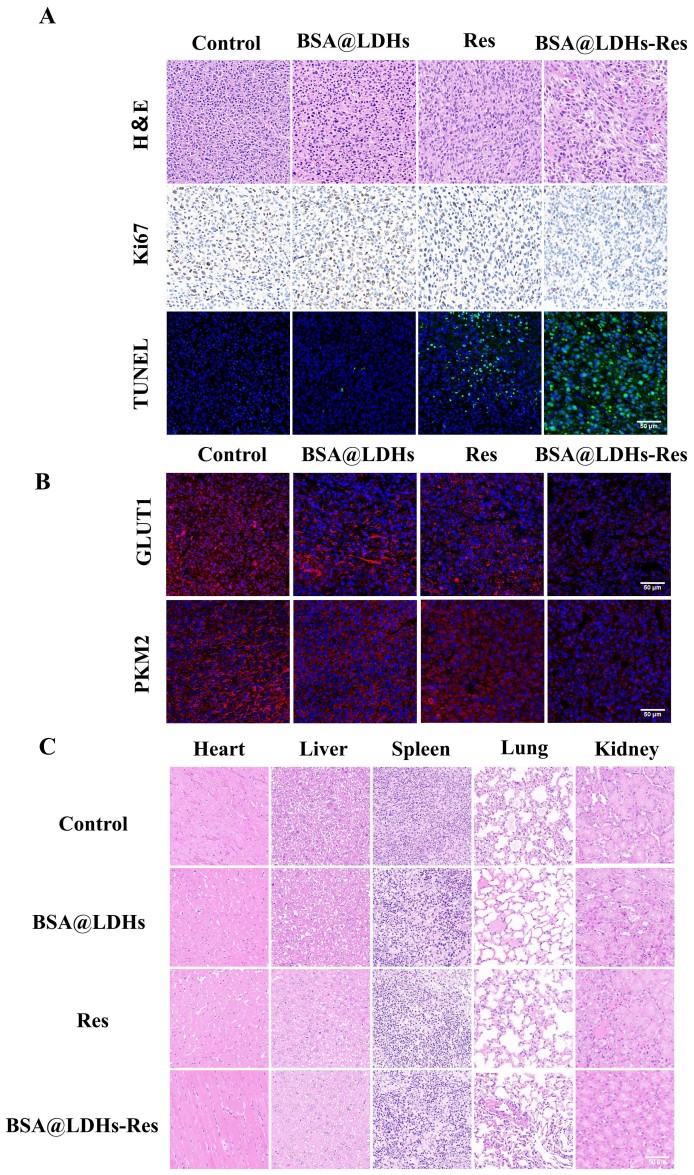

Figure 8 (**A**) H&E, ki67, and TUNEL staining results of tumor sections from different treatment groups; (**B**) GLUT1 and PKM2 immunofluorescence results of tumor sections from different treatment groups; (**C**) H&E staining images of organs such as heart, liver, spleen, lungs, and kidneys treated with different materials. Scale bar: 50μm.

glucose transporter protein.[21,22] Through targeted inhibition of key enzymes and regulatory factors, glycolysis in cancer cells can be blocked, leading to cancer cell death. Therefore regulating aerobic glycolysis in breast cancer cells is a very promising therapeutic strategy. Breast cancer cells exhibit enhanced glycolysis and altered glucose metabolism.

Resveratrol, a naturally occurring polyphenol, has been extensively studied in clinical trials for its potential role in cancer treatment.[23] Resveratrol is known for its ability to modulate various cellular processes, and one of its mechanisms of action involves the inhibition of glycolysis in cancer cells. Studies have shown that resveratrol can effectively inhibit the growth of non-small cell lung cancer (NSCLC) cells, and high concentrations of resveratrol can regulate the protein kinase B (Akt) signaling pathway, leading to the downregulation of hexokinase 2 (HK2) expression, thereby slowing the rate of glycolysis resveratrol can suppress the activity of 6-phospho-fructo-1-kinase (PFK), a key regulatory enzyme in the glycolytic pathway.[24] However, resveratrol has poor solubility and bioavailability. To address the stability and solubility issues of resveratrol, resveratrol nanoparticles have emerged as a promising therapeutic strategy in the treatment of various cancers. Jia et al have developed pH

and redox-responsive micellar complexes that co-deliver PD-L1 siRNA and resveratrol, effectively balancing the glycolytic and oxidative phosphorylation pathways in tumor cells and reversing the immunosuppressive tumor microenvironment. The co-delivery of PD-L1 siRNA and resveratrol via these micelles enhances the antitumor activity of immune cells within the tumor microenvironment, thereby boosting the effectiveness of PD-L1 immunotherapy.[25] Additionally, gold nanomaterials prepared with resveratrol and polydopamine have been studied for their cancer treatment applications, particularly their impact on tumor glycolysis.[26] These nanoscale gold particles loaded with resveratrol (Res-GNPs) exhibit enhanced antitumor activity compared to free resveratrol. Collectively, these findings demonstrate the potential of resveratrol-loaded nanomaterials in inhibiting tumor glycolysis, offering novel perspectives and approaches for cancer therapeutics.

BSA-modified LDHs loaded with drugs have become a nanomaterial with great potential in enhancing drug delivery efficiency and therapeutic outcomes, especially showing significant prospects in the field of cancer treatment.[27] Firstly, these nanoparticles demonstrate good dispersibility in environments similar to those within the body due to surface BSA modification. Secondly, LDHs can respond to changes in the microenvironment, such as slight acidity, achieving controlled drug release and exhibiting environmental responsiveness. The biodegradability of LDHs ensures no significant toxic side effects when applied reasonably and can degrade and be expelled in a timely manner after functioning, reducing the risk of long-term accumulation.[28] Recent studies have used bovine serum albumin-coated layered double hydroxides (BSA-LDHs) to encapsulate resveratrol. In the supramolecular complex formed with LDH, resveratrol will be placed in the interlayer region of LDHs, stabilized by intermolecular interactions. The study evaluated the anticancer ability of the nanoformulation in a human lung cancer cell line (A549), showing higher activity than free drug alone.[19] However, this study did not explore whether the albumin-modified layered double hydroxides exhibit better pharmacological effects than the single drug in animal experiments, nor did it investigate whether this drug formulation exerts antitumor effects by inhibiting the glycolysis pathway.

In this study, an albumin-modified layered double hydroxide piggybacked resveratrol nanocarrier system was successfully prepared. Breast cancer cells internalized BSA@LDHs-Res by endocytosis, which increased the permeability of the lysosomal membrane and evaded lysosomal trapping. After entering the cells, BSA@LDHs-Res first inhibited the expression of GLUT1, reduced the glucose entering the cells, and blocked the supply of energy upstream of glycolysis. At the same time, BSA@LDHs-Res inhibited the expression and activity of the key enzymes of glycolysis, HK2, PKM2 and LDH, resulting in decreased glucose consumption, decreased lactate accumulation and decreased intracellular ATP levels. BSA@LDHs-Res inhibited the proliferation of breast cancer cells, SKBR3 and MDA-MB-231, more efficiently and stably by regulating aerobic glycolysis, migration and invasion. In addition, it induced changes in mitochondrial membrane potential, promoted ROS generation, and facilitated apoptosis. In the evaluation of the in vivo mouse model, the nanoformulation of resveratrol modified with bovine serum albumin-layered double hydroxides (BSA-LDHs) also showed good antitumor effects. Compared to the groups treated with BSA-LDHs alone and resveratrol alone, it significantly inhibited tumor growth, with no obvious changes in body weight and no significant toxicity to the heart, liver, spleen, lungs, and kidneys of the mice, indicating good drug safety. More importantly, the levels of GLUT1 and PKM2 in the tumors of mice treated with the BSA-LDHs-Res nanoformulation were lower than in other treatment groups, reflecting that the resveratrol nanoformulation modified with bovine serum albumin-layered double hydroxides has superior energy consumption capabilities compared to other formulations. (Scheme 1). In this article, although we utilized resveratrol encapsulated in albumin-modified layered double hydroxides to inhibit the growth of breast cancer by suppressing glycolysis pathways, there are still some issues worth further explore. For example, while LDHs are generally biocompatible, the long-term effects and potential toxicity of these materials in vivo need thorough investigation. There is a risk that the body could develop an immune response to the LDHs, which could limit its therapeutic application. In summary, although BSA-LDHs nanomaterials have shown potential in the delivery of resveratrol, there are still many scientific questions that need to be addressed through further research. These studies will help to enhance the effectiveness and safety of BSA-LDHs nanomaterials in cancer treatment.

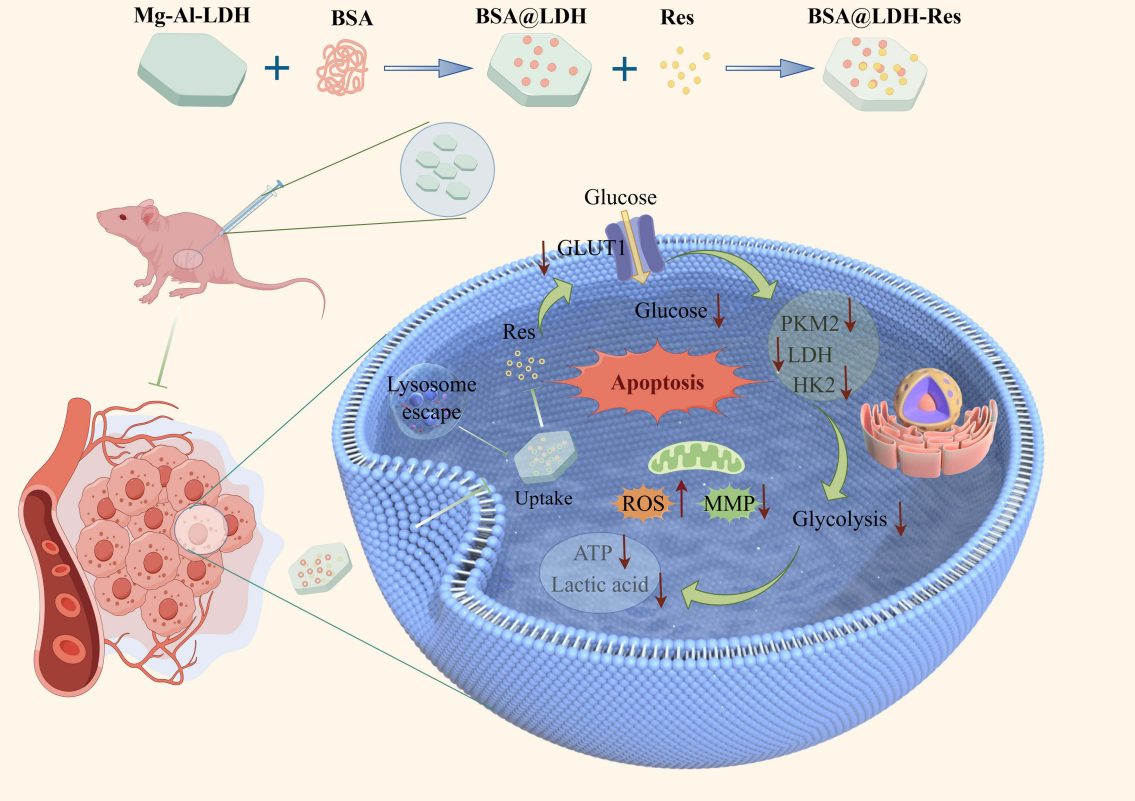

Scheme 1 Schematic representation of the BSA@LDHs-Res nanodelivery system for the treatment of breast cancer.

Conclusion

In this study, we constructed a new albumin-modified BSA@LDHs-Res drug-carrying dosage form, and BSA@LDHs-Res was able to accurately control the drug release due to the pH sensitivity of the lamellae, reduce the expression of GLUT1, cut off the supply of glucose, and block the supply of energy upstream of glycolysis. By inhibiting the activity and expression of key enzymes of glycolysis to regulate the glycolysis of breast cancer cells, the anti-breast cancer effect can be achieved. The albumin-modified resveratrol layered double hydroxide delivery system developed in this study will provide certain theoretical references for further research and clinical application of tumor aerobic glycolysis.

Ethical Approval

This animal experiment was reviewed and approved by the Anhui Provincial Laboratory Animal Management and Ethics Committee and the Ethics Committee of Bengbu Medical university, Ethics No. [2022] No. 147. All experiments were conducted in accordance with the Regulations for the Management of Animals and the Implementing Rules for the Management of Medical Laboratory Animals.

Funding

This work was supported by the The Natural Science General Project of Bengbu Medical University(2024byzd033),the Anhui Province New Era Graduate Academic Innovation Project under the Provincial Quality Engineering Program (2024xscx137), the University Synergy Innovation Program of Anhui Province (GXXT-2022–064), the Excellent Scientific Research and Innovation Team of Anhui Universities(2024AH010021)the Natural Science Key Program of Bengbu Medical University (2022byzd022), and the National Student Innovation and Entrepreneurship Training Program Project of Bengbu Medical University (202410367004).

Disclosure

The authors declare that they have no known competing financial interests or personal relationships that could have appeared to influence the work reported in this paper.

References

1. Zheng RS, Chen R, Han BF, et al. Cancer incidence and mortality in China, 2022. *Zhonghua Zhong Liu Za Zhi*. 2024;46(3):221–231. doi:10.3760/cma.j.cn112152-20240119-00035
2. Corti C, Giugliano F, Nicolò E, Tarantino P, Criscitiello C, Curigliano G. HER2-low breast cancer: a new subtype? *Curr Treat Options Oncol*. 2023;24(5):468–478. doi:10.1007/s11864-023-01068-1
3. Hermansyah D, Firsty NN, Siagian RHN, Dwinda NN. Intercontinental comparison of immunohistochemical subtypes among individuals with breast cancer in South-East Asia and South America: a scoping systematic review and meta-analysis of observational studies. *World J Oncol*. 2024;15(3):355–371. doi:10.14740/wjon1788
4. Wang N, Ma T, Yu B. Targeting epigenetic regulators to overcome drug resistance in cancers. *Signal Transduct Target Ther*. 2023;8(1):69. doi:10.1038/s41392-023-01341-7
5. Zhao J, Sun H, Wang C, Shang D. Breast cancer therapy: from the perspective of glucose metabolism and glycosylation. *Mol Biol Rep*. 2024;51(1):546. doi:10.1007/s11033-024-09466-w
6. Huang Y. Targeting glycolysis for cancer therapy using drug delivery systems. *J Control Release*. 2023;353:650–662. doi:10.1016/j.jconrel.2022.12.003
7. Qingdong GAO, Xufang DUAN, Yan LI, et al. Research on the role of resveratrol against breast cancer[J]. *ZHONGGUO YAOFANG*. 2024;35(11):1408–1412. doi:10.6039/j.issn.1001-0408.2024.11.22
8. Ho Y, Li ZL, Shih YJ, et al. Integrin αvβ3 in the mediating effects of dihydrotestosterone and resveratrol on breast cancer cell proliferation. *Int J mol Sci*. 2020;21(8):2906. doi:10.3390/ijms21082906
9. Wu Q, Zhao B, Sui G, Shi J. Phytochemicals block glucose utilization and lipid synthesis to counteract metabolic reprogramming in cancer cells. *Appl Sci*. 2021;11(3):1259. doi:10.3390/app11031259
10. Behroozaghdam M, Dehghani M, Zabolian A, et al. Resveratrol in breast cancer treatment: from cellular effects to molecular mechanisms of action. *Cell mol Life Sci*. 2022;79(11):539. doi:10.1007/s00018-022-04551-4
11. Wu Z, Wu J, Zhao Q, Fu S, Jin J. Emerging roles of aerobic glycolysis in breast cancer. *Clin Transl Oncol*. 2020;22(5):631–646. doi:10.1007/s12094-019-02187-8
12. Bhaskara VK, Mittal B, Mysorekar VV, Amaresh N, Simal-Gandara J. Resveratrol, cancer and cancer stem cells: a review on past to future. *Curr Res Food Sci*. 2020;3:284–295. doi:10.1016/j.crfs.2020.10.004
13. Cecerska-Heryć E, Wiśniewska Z, Serwin N, et al. Can compounds of natural origin be important in chemoprevention? Anticancer properties of quercetin, resveratrol, and curcumin-a comprehensive review. *Int J mol Sci*. 2024;25(8):4505. doi:10.3390/ijms25084505
14. Tan Y, Feng J, Xiao Y, Bao C. Grafting resveratrol onto mesoporous silica nanoparticles towards efficient sustainable immunoregulation and insulin resistance alleviation for diabetic periodontitis therapy. *J Mater Chem B*. 2022;10(25):4840–4855. doi:10.1039/d2tb00484d
15. Wang W, Zhang L, Chen T, et al. Anticancer effects of resveratrol-loaded solid lipid nanoparticles on human breast cancer cells. *Molecules*. 2017;22(11). doi:10.3390/molecules22111814
16. Pang S, Geng C, Fan Z, et al. Synergistic effect of layered double hydroxides nanodosage form to induce apoptosis and ferroptosis in breast cancer. *Int J Nanomed*. 2024;19:4199–4215. doi:10.2147/ijn.S455427
17. Wang H, Jing G, Niu J, et al. A mitochondria-anchored supramolecular photosensitizer as a pyroptosis inducer for potent photodynamic therapy and enhanced antitumor immunity. *J Nanobiotechnology*. 2022;20(1):513. doi:10.1186/s12951-022-01719-9
18. Wang Z, Xu Z, Jing G, et al. Layered double hydroxide eliminate embryotoxicity of chemotherapeutic drug through BMP-SMAD signaling pathway. *Biomaterials*. 2020;230(119602):119602. doi:10.1016/j.biomaterials.2019.119602
19. Minnelli C, Laudadio E, Galeazzi R, et al. Encapsulation of a neutral molecule into a cationic clay material: structural insight and cytotoxicity of resveratrol/layered double hydroxide/BSA nanocomposites. *Nanomaterials (Basel)*. 2019;10(1):33. doi:10.3390/nano10010033
20. Gansler T, Ganz PA, Grant M, et al. Sixty years of CA: a cancer journal for clinicians. *CA Cancer J Clin*. 2010;60(6):345–350. doi:10.3322/caac.20088
21. Ciavardelli D, Rossi C, Barcaroli D, et al. Breast cancer stem cells rely on fermentative glycolysis and are sensitive to 2-deoxyglucose treatment. *Cell Death Dis*. 2014;5(7):e1336. doi:10.1038/cddis.2014.285
22. Pelicano H, Martin DS, Xu RH, Huang P. Glycolysis inhibition for anticancer treatment. *Oncogene*. 2006;25(34):4633–4646. doi:10.1038/sj.onc.1209597
23. Kursvietiene L, Kopustinskiene DM, Staneviciene I, et al. Anti-cancer properties of resveratrol: a focus on its impact on mitochondrial functions. *Antioxidants (Basel)*. 2023;12(12). doi:10.3390/antiox12122056
24. Gomez LS, Zancan P, Marcondes MC, et al. Resveratrol decreases breast cancer cell viability and glucose metabolism by inhibiting 6-phosphofructo-1-kinase. *Biochimie*. 2013;95(6):1336–1343. doi:10.1016/j.biochi.2013.02.013
25. Jia L, Gao Y, Zhou T, et al. Enhanced response to PD-L1 silencing by modulation of TME via balancing glucose metabolism and robust co-delivery of siRNA/Resveratrol with dual-responsive polyplexes. *Biomaterials*. 2021;271(120711):120711. doi:10.1016/j.biomaterials.2021.120711
26. Zhang D, Zhang J, Zeng J, et al. Nano-gold loaded with resveratrol enhance the anti-hepatoma effect of resveratrol in vitro and in vivo. *J Biomed Nanotechnol*. 2019;15(2):288–300. doi:10.1166/jbn.2019.2682
27. Zuo H, Chen W, Cooper HM, Xu ZP. A facile way of modifying layered double hydroxide nanoparticles with targeting ligand-conjugated albumin for enhanced delivery to brain tumour cells. *ACS Appl Mater Interfaces*. 2017;9(24):20444–20453. doi:10.1021/acsami.7b06421
28. Li L, Qian Y, Sun L, et al. Albumin-stabilized layered double hydroxide nanoparticles synergized combination chemotherapy for colorectal cancer treatment. *Nanomedicine*. 2021;34(102369). doi:10.1016/j.nano.2021.102369